Supporting Information

SnO_2@Carbon Nanocluster Anode Material with Superior Cyclability and Rate Capability for Lithium-Ion Batteries

Min He, [a, b] *Lixia Yuan,* [a,*] *Xianluo Hu,* [a] *Wuxing Zhang,* [a] *Jie Shu* [c] *and Yunhui Huang* [a,*]

[a] *Key Laboratory for Advanced Battery Materials and System, Ministry of Education; School of Materials Science and Engineering, Huazhong University of Science and Technology (HUST), Wuhan 430074, China*

[b] *School of Science, Wuhan University of Science and Technology, Wuhan 430065, China*

[c] *Faculty of Materials Science and Chemical Engineering, Ningbo University, Ningbo, 315211, China.*

Corresponding author. E-mail addresses:

yuanlixia@mail.hust.edu.cn(L.X. Yuan), huangyh@mail.hust.edu.cn (Y. H. Huang).

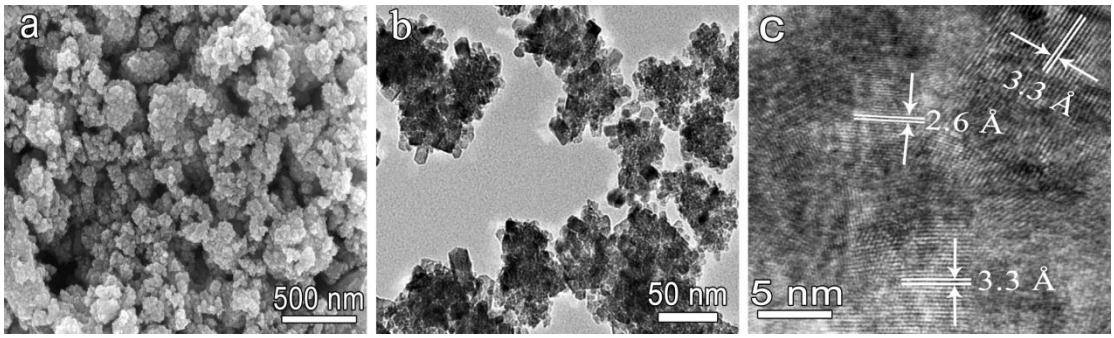

Fig. S1 (a) SEM, (b) TEM and (c) HRTEM images of bare SnO_2 nanoparticles.

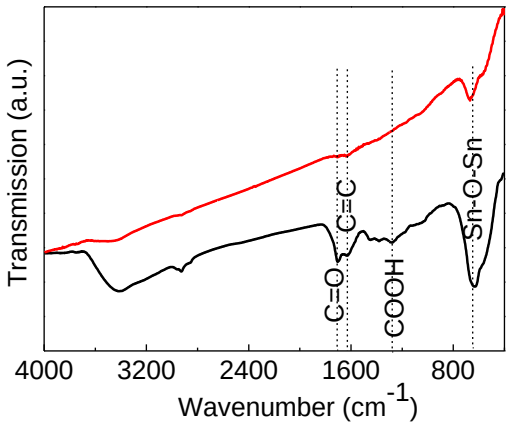

Fig. S2 Infrared spectra of SnO_2@C before (black curve) and after calcination (red curve).

In order to confirm the existence of carbon, FTIR spectrum was employed to measure the prepared nanoclusters before (black curve) and after (red curve) calcination in Fig. S2. It can be seen that the strong absorption peak at 640 cm^{-1} of the two samples can be attributed to the stretching vibration of Sn-O-Sn, which stem from the SnO_2 in the composite products. From absorption curve before calcination, the peak around 1703 cm^{-1} and 1278 cm^{-1} are owed to C=O vibration and the carboxyl functional group [16], respectively, other two weak peaks at 2923 cm^{-1} and 1452 cm^{-1} were regarded as saturated hydrocarbon absorption, indicating the presence of carbon with rich organic functional groups.[14] In addition, the other peak at 3400 cm^{-1}, 1635cm^{-1} and 1368 cm^{-1} were related to the hydroxyl vibrations due to absorbed water on the surface of the nanopowders. Obviously, most of these peaks disappear after carbonization according to the red curve in Fig. S2, which indicates the full transformation from the carbonaceous layer to carbon by thermal treatment.

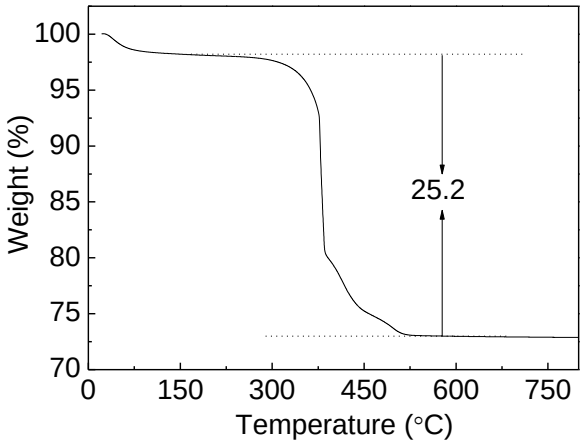

Fig. S3 TGA curves for SnO_2@C nanoclusters.

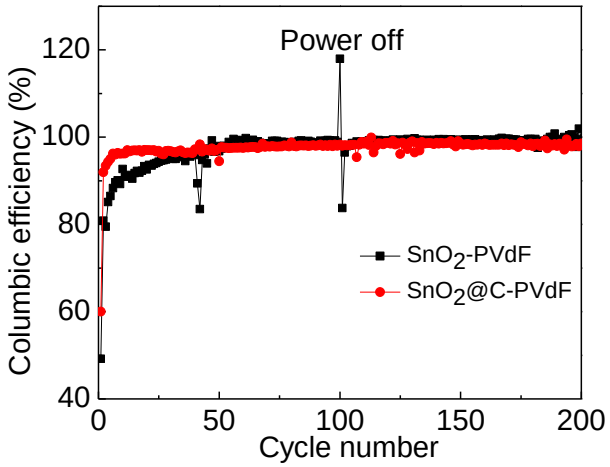

Fig. S4 Columbic efficiency of the bare SnO_2-PVDF and SnO_2@C-PVDF electrode at the potential window of 2.5–0.01 V and at the current density of 100 mA g^{-1}.

The two anodes show different columbic efficiency. Before 50 cycles, the columbic efficiency of the SnO_2@C-PVDF electrode is obviously higher than that of bare SnO_2-PVDF electrode. Typical, the columbic efficient of bare SnO_2-PVdF electrode rise from ~80% in the second cycle to 90% in the 10^{th} cycle, then slowly increase to 97% before the 50th cycle, and basically stabilize over ~98% after that. In contrast, for the SnO_2@C-PVDF electrode, the columbic efficient attain above 90% in the second cycle, then increase to 95% in 5^{th} cycle and stabilize at ~98% after the 100th cycle. The stable

columbic efficient of the SnO_2@C-PVDF electrode may be due to relatively low volume change from the carbon shell buffering, producing the less new formed surface area of the anodes during the charge/discharge process, decreasing the side reactions between the anodes and the electrolyte compared to that of the bare SnO_2-PVDF electrode. Therefore, the SnO_2@C-PVDF electrode exhibits stable columbic efficiency.

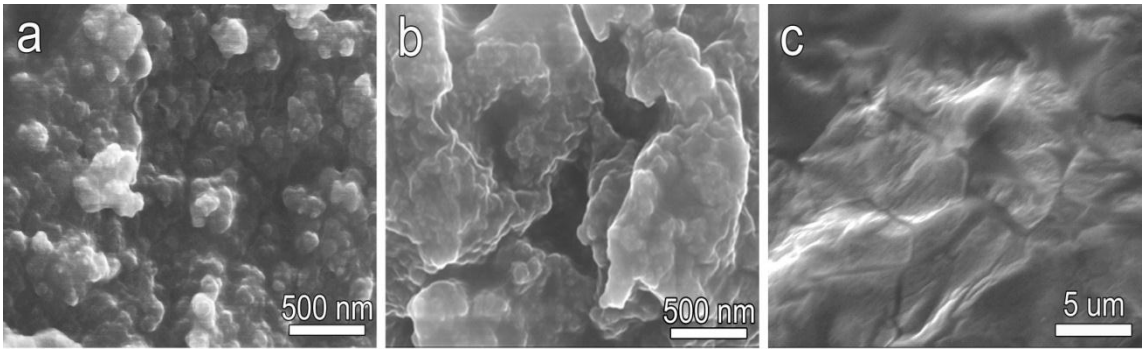

Fig. S5 Ex-situ SEM images of the other electrode after 200 cycles: (a) SnO_2@C-PVDF electrode, (b) SnO_2-CS electrode, and (c) SnO_2-PVDF electrode.